# Measurement and calculation of the pressure dependence of the Mössbauer isomer shift of metallic $^{119}$Sn for the pressure range $0 \leq P \leq 310$ kbar

Lee Chow,* Phillip A. Deane,† Joseph N. Farrell,‡ Paul A. Magill, and Louis D. Roberts
*Department of Physics and Astronomy, University of North Carolina, Chapel Hill, North Carolina 27514*
(Received 10 June 1985; revised manuscript received 15 October 1985)

We have measured the pressure dependence of the Mössbauer isomer shift $S(P)$ for tin for the pressure range $0 \leq P \leq 310$ kbar through the use of a diamond anvil pressure cell. Also, $S(P)$ has been calculated for this pressure range using a relativistic augmented-plane-wave model. In these calculations, a Kohn-Sham, a Hedin-Lundqvist, or a Slater model was used to describe the electron-electron interaction. A Dirac-Hartree-Wigner-Seitz model was used to calculate the muffin-tin potential. For the 92-kbar phase transition, the calculated change of the electron density at the tin nucleus was found to be roughly independent of whichever of the above models was used to describe the electron many-body interaction. Based on this, a value for the Mössbauer isomer-shift calibration constant of $0.072 a_0^3$ mm/sec, and an approximate description of the measured $S(P)$ for the above pressure range is obtained. A comparison of our results with other measurements and calculations is made.

## I. INTRODUCTION

We have measured the pressure dependence of the Mössbauer isomer shift,[1] $S(P)$, for tin. $S(P)$ is proportional to a difference of electron densities at the tin nucleus. We will define this difference below. Our measurements of $S(P)$ have been made for pressures $P$ in the range 0—310 kbar. For this range of pressure, the bulk density of tin increases by about 30%, and there is a change of phase near 92 kbar.[2–4]

The electron-electron interaction in a solid is a function of the distance between the electrons. Thus a study of the pressure, or electron density, dependence of some suitable solid-state property may provide a useful way to study this interaction. In several recent papers[5–7] we have suggested that the study of the pressure dependence of the Mössbauer isomer shift for tin may be suitable for this purpose.

Here, we seek to explore the possible sensitivity of $S(P)$ for Sn to the mathematical model used to describe the electron many-body interaction, through measurements,[8] and through several relativistic augmented-plane-wave (RAPW) calculations[8] of the pressure dependence of the Mössbauer isomer shift. We have made the RAPW calculations of $S(P)$ for the above pressure range, $0 \leq P \leq 310$ kbar, and for several different approximate treatments of the electron many-body interaction.

Earlier measurements of $S(P)$ for tin to about 100 kbar have been made by Möller[9,10] and Mössbauer,[10] and measurements to a pressure of about 130 kbar have been made by Panyushkin[11,12] and by Panyushkin and Voronov.[12] Earlier calculations of $[dS(P)/dP]_0$ at $P=0$ have been made by Inglesfield,[13] Antoncik,[14] Williamson *et al.*,[5] Krakow *et al.*,[6] and by Page *et al.*,[7] but no previous calculation of $S(P)$ as a function of $P$ through the 92-kbar phase transition and to higher pressures has been made.

In the earlier Mössbauer studies of the low-pressure phase of tin,[9–12] the isomer shift $S(P)$ was found to decrease with increasing $P$. Here, $[dS(P)/dP]_0 < 0$. This behavior was found to correspond to a decrease (rather than to the increase one might expect) of the electron density at the nucleus as the pressure $P$, and the bulk metallic density, are increased. The several calculations[5–7,13,14] of this derivative mentioned above are in qualitative accord with this result. The dependence, for tin, of the sign and magnitude of the slope of $S(P)$, with increasing $P$, on the treatment of exchange and correlation are the primary subject of this paper.

### A. A qualitative discussion of the sign and magnitude of $[dS(P)/dP]_0$

One may perhaps most easily see why the electron density at a nucleus might decrease as the density of the solid is increased, or as the atomic or Wigner-Seitz volume $V$ is decreased, by considering the following picture. Imagine, say, a cubic close-packed lattice of hydrogen atoms of infinite-lattice parameter. At infinite-lattice parameter, the electron density at or near a nucleus would be the same as for a free hydrogen atom. When $V$ is decreased to a large but finite value, in a linear combination of atomic orbitals (LCAO) model, the amplitude of the wave function in the overlap region between the atoms would be expected to increase faster than the amplitude near a nucleus. In the normalized wave function, and at very large $V$, as $V$ is decreased electron density will move away from the nuclei into the overlap region, and the electron density at a nucleus will decrease as the density of the solid is increased. When the atoms are brought quite close together, however, in the LCAO model, this trend will reverse and the electron density near a nucleus and the bulk density of this supposed hydrogen solid will be expected to increase together. In this LCAO picture for hydrogen, there would be a minimum in a plot of the electron density at the nucleus versus $1/V$.

Because a more exact treatment of even this hydrogen

 

problem is complex, some years ago, we felt that it might be useful to make a preliminary, exploratory study of the systematic behavior of the electron density at the nucleus, $\rho_{VZ}(0)$, as a function both of $1/V$ and of the atomic number $Z$, in a Dirac-Hartree-Wigner-Seitz-XC (DHWSXC) model.[15] Here, XC refers to the fact that the model includes a description of exchange and correlation in the form of a local potential. We will describe some details of this DHWSXC model below in Sec. IV D.

For the moment, however, as is suggested by the LCAO picture above, a minimum of $\rho_{VZ}(0)$ as a function of $1/V$ is found for hydrogen in the DHWSXC model also. This predicted minimum was found to occur at a Wigner-Seitz radius near 1.1 a.u.[15] The hydrogen lattice imagined above, however, does not exist in the laboratory.

When $\rho_{VZ}(0)$ was calculated as a function of $1/V$ for the elements[5-7] in the DHWSXC model, a somewhat more complex behavior than that for hydrogen was found for values of $Z$ near the inert gases. For each element, $1 \leq Z \leq 92$, however, there was a value for $1/V = 1/V_m$ at which a minimum, similar to that suggested above, was found to occur. The reciprocal atomic volume for an element is a function of the pressure, $1/V = 1/V(P)$. The sign of $[dS(P)/dP]_0$ predicted by the model for an element will thus depend on whether the normal reciprocal atomic volume of the element $1/V(0)$, at $P = 0$, is above or below the value of $1/V_m$ for the element.

For the transition and rare-earth elements, the minimum is found to occur at a value for $1/V_m$ well below $1/V(0)$ for the element. Here, one would expect the electron density at the nucleus to increase when the solid is compressed.[7]

For the *sp* metals of the periodic table, however, this minimum was found to occur at a $1/V_m$ value in the vicinity of $1/V(0)$ for each of them. For example, for Ag the minimum was at a value of $1/V_m$, which was well below $1/V(0)$. For tin and antimony, however, the value of $1/V_m$ was quite near to the respective $1/V(0)$ values. For these elements, near their normal bulk metallic densities, the DHWSXC model thus predicts that the electron density at the nucleus should increase for Ag, that it would change but slightly for Sn, but that it should decrease slowly for Sb with increasing $1/V(P)$ (see Sec. V E). These minima are described in some detail in several earlier papers.[5-7,15]

As a result of these calculations, we measured $S(P)$ and $[dS(P)/dP]_0$ for Sb for $0 \leq P \leq 70$ kbar.[6,17,18] These results were found to be in qualitative accord with the DHWSXC model.[6]

An accurate description of the properties of $\rho_{VZ}(0)$ and of $S(P)$, such as those qualitatively depicted above, will depend on the crystal structure and on the nature of the bonding as well as on electron screening effects in the solid. The DHWSXC model which we have used above is only a partial treatment of this problem, but it may serve[7] to indicate the systematic behavior of $\rho_{VZ}(0)$ with $Z$ and $1/V(P)$. As we have noted, the model contains a description of the electron-electron interaction.

In these DHWSXC-model studies it was found that, for the *sp* metals, the value of $1/V_m$ at which a minimum of $\rho_{VZ}(0)$ would occur depended, not only on the element $Z$, but also on the description of the many-body interaction used.[5-7] Calculations of $\rho_{VZ}(0)$ were made for the Kohn-Sham[19] (KS), Hedin-Lundqvist[20] (HL), and for the Slater[21] (SR) treatments of exchange and correlation. It was found that for a given element and for the sequence KS, HL, to SR, the minimum moved to higher values of $1/V_m$. This would correspond to a less positive or to an increasingly negative value for $[d\rho_{VZ}(0)/dP]_0$, for this sequence of descriptions of exchange and correlation. This implies that information about exchange and correlation is contained in the slope of the isomer shift[5-7] $S(P)$ with increasing $P$.

This qualitative DHWSXC survey of the systematic behavior of $\rho_{VZ}(0)$ with $Z$ and $1/V$ suggested that tin might be a particularly suitable element for a more detailed study of the dependence of $S(P)$ and of $[dS(P)/dP]_0$ on the many-body potential.[5-7] From the DHWSXC-model studies of $[d\rho_{VZ}(0)/dP]_0$ as a function of $Z$, $[dS(P)/dP]_0$ for tin was predicted to have a relatively small value, and the model indicated that, for the sequence of interactions, KS, HL, to SR larger fractional changes of the value of this derivative might be expected than for other Mössbauer elements. The above survey together with considerations of experimental properties, Sec. II A, led to the present measurements and calculations of $S(P)$ for tin.

### B. The present study

Returning now to the present work, we seek to continue the study of the dependence of $S(P)$ for tin on the many-body potential. To this end, we have (a) made a more detailed measurement of $S(P)$ for tin for a wider range of pressure and metallic density[8] than was available from earlier experiments, and (b) we describe a RAPW calculation[8] of $S(P)$. In comparison with the DHWSXC model, this RAPW calculation should provide an improved description of the dependence of $S(P)$ on $1/V(P)$ and on exchange and correlation.

The RAPW calculations of $S(P)$ have been made for the pressure range, $0 \leq P \leq 310$ kbar, for the two tin phases, and for the KS, HL, and the SR treatments of the electron-electron interaction. In these calculations, apart from the description of the electron many-body interaction, the RAPW programs used for the several calculations were the same. Thus, for the sequence of interactions, KS, HL, to SR, an indication is obtained in the RAPW model of the trend with, and of the sensitivity of the calculated $S(P)$ to, the description of exchange and correlation.[8]

A comparison of these calculated $S(P)$ curves with the experimental $S(P)$ data can indicate whether the changes of the calculated $S(P)$ curves between the KS, HL, and SR treatments of exchange and correlation are comparable to, or larger than, the experimental errors in the measured $S(P)$. This comparison may give a further indication, beyond our earlier DHWSXC calculations, as to whether the measured $S(P)$ and $[dS(P)/dP]_P$, for tin, contain information about exchange and correlation in a form which is useful and accessible to an experimental study. The contributions to $S(P)$ from the core states and

from the valence-band states, at the phase transition and as a function of $P$, are estimated. As an aspect of this comparison of the measured with the calculated $S(P)$, an estimate is made of the Mössbauer isomer-shift calibration constant and of the change of the $^{119}$Sn nuclear size when a Mössbauer gamma-ray quantum is absorbed.[8] Also, we were interested to see whether a minimum in $\rho_{VZ}(0)$ as a function of $P$, or of $1/V(P)$, would occur within the pressure range of the present study.

## II. HIGH-PRESSURE ISOMER-SHIFT EXPERIMENTS

The Mössbauer isomer shift for tin is described by the relations[1,16]

$$S(P)=(2\pi/3)(c/E_\gamma)Ze^2\Delta\langle r^2\rangle g\Delta\rho_P(0) \quad (1a)$$

$$=\alpha g\Delta\rho_P(0) \quad (1b)$$

$$=\alpha g[\rho_P(0)-\rho_Q(0)] . \quad (1c)$$

Here, $c$ is the velocity of light, $E_\gamma$ is the energy of the Mössbauer $\gamma$ ray, $Ze$ is the nuclear charge, and $\Delta\langle r^2\rangle$ is the change of the nuclear mean-square charge radius which occurs when the resonance $\gamma$ ray is absorbed. $\rho_P(0)$ is the electron density at $r=0$, viz., at the center of a tin nucleus at a pressure $P$. $\Delta\rho_P(0)$ is the difference between the total electron density at $r=0$ within a tin nucleus in the Mössbauer absorber at a pressure $P$ and this electron density at a selected reference pressure $Q$. $g$ is the factor by which we multiply $\Delta\rho_P(0)$ to obtain the difference of the electron densities averaged over the nuclear volume. $\alpha$ is the Mössbauer isomer-shift calibration constant. In the following, we will use $Q=90$ kbar as the reference pressure. $g$ will be found to have a value $g=0.975$. The measurements were made at ambient temperature, 294–298 K.

### A. The metallic tin Mössbauer absorber

There are several experimental reasons why metallic tin is suitable for this study of $S(P)$ in which a diamond anvil high-pressure clamp was used. Among the elements, tin is relatively highly compressible[2–4,22] and has a phase transition within our pressure range.[4] With its comparatively large cross section for the recoilless radiation process,[23] Sn is one of the better elements for Mössbauer isomer-shift measurements. The quadrupole splitting of the Mössbauer spectrum is small,[24,25] only of the order of the natural line width.[23] This is helpful because a large quadrupole splitting, in the presence of the pressure gradients which may occur in the high-pressure cell, could make it more difficult[26] to measure $S(P)$. As a result of the above, even with the quite small Mössbauer absorber sample size that is available with a diamond high-pressure clamp, it was possible to measure $S(P)$ with a relatively small statistical error.

### B. The diamond anvil cell

The diamond anvil cell which we have used for these measurements is similar in design to a cell described by Block and Piermarini.[27] All components of our cell were fabricated from the maraging steel, Vascomax 300. The diamonds used in this work ranged in size from $\frac{1}{4}$ to $\frac{1}{3}$ carat and were of the standard brilliant cut. An anvil high-pressure face was prepared by polishing off the culet of a diamond to give an anvil face diameter in the range of about 0.75 to 1.00 mm. We obtained pressures to 195 kbar with diamonds with anvil face diameters near 1.00 mm. To obtain higher pressures, smaller anvil face diameters were used.

The tin Mössbauer sample was contained in the central hole of a gasket, about 0.05 to 0.1 mm thick, which was clamped between diamond anvils. The gasket hole ranged in size from about 0.2 to 0.45 mm. The tin sample was in the form of a small disk which was cut, or punched, to fit the gasket hole closely. The tin sample thickness was in the vicinity of 0.01 to 0.03 mm. In most cases, the sample was prepared from tin of the naturally occuring isotopic abundance, although, in several cases, a sample containing 96% $^{119}$Sn was used. A 4:1 methanol-ethanol or a 16:3:1 methanol-ethanol-water mixture was used as the pressure-transmitting medium.[28]

The above gasket served two purposes. It served to contain the tin sample at high pressures, and it also served as a collimator for the 23.9 kev $^{119}$Sn Mössbauer $\gamma$ rays. For the latter purpose, it was essential to use a gasket material of high-electron density. W, Mo, and Re gaskets were successfully used. Re was perhaps the best gasket material. Of these elements, it has the highest atomic number and density. Also, under pressure, Re seemed to bond to the diamond anvil faces to some degree, and, in comparison with W or Mo, the gasket hole diameter increased but little as the pressure on the sample was increased.

### C. Pressure measurements

The pressure in the sample chamber was measured by the ruby fluorescence method.[27–29] Several chips of ruby, about 0.025 mm in size, were placed in the gasket hole along with the Sn sample and in the pressure transmitting medium. The pressure was measured at each ruby chip. A He-Cd laser was used to excite the red ruby emission lines, and the wavelength shift with pressure of the $R_1$ line, $\Delta\lambda(P)$, was measured. Pressures were then obtained from the formula of Mao *et al.*[29] With $\Delta\lambda(P)$ in Angstroms,

$$P=3808\{[\Delta\lambda(P)/(6942\ \text{Å})+1]^5-1\}\ \text{kbar} . \quad (2)$$

Near or below about 100 kbar, the pressures measured at the several ruby chips agreed within a few kbar. Near 300 kbar, the agreement was within a range of about 10% of $P$, or better. The average of the pressures measured for the several chips was assumed to describe the pressure in the cell.

### D. Mössbauer measurements

The Mössbauer measurements were made with an apparatus which was closely similar to equipment which we have described previously.[6,26] In each experiment, a measurement of the six-line spectrum of $\alpha$-iron was made simultaneously with the measurement of the Sn

Mössbauer spectrum. This provided a precise velocity calibration, individually, for each tin spectrum measurement. For the Sn spectra, calcium stannate Mössbauer sources with activities of 0.7—4 mci were used. Depending on various factors, the tin $\gamma$ ray counting rate was 20—60 $sec^{-1}$. The counting time for a measurement of $S(P)$ was one to two weeks. Both the tin and the $\alpha$-iron spectra were analyzed with a least-squares Lorentz curve fitting computer program.[30,31] A single Lorentz line-shape function was fitted to each individual Fe line. The Sn spectrum consists of an unresolved quadrupole pair of absorption lines.[24] We fitted a single Lorentz line-shape function to the data for this unresolved quadrupole pair. The velocity corresponding to the center of this single fitted Lorentz line function, when suitably corrected for geometry effects, was taken to describe the tin isomer shift.

### E. Corrections to the measured data

We have made estimates of possible corrections to this measured isomer shift due to the second-order Doppler shift,[1] and due to the pressure dependence of the splitting, and relative line intensities, of the components of the quadrupole pair.[24] We find that the corrections to the measured isomer shift, above, due to these effects, may be expected to be smaller than our error of measurement of about 0.01 to 0.02 mm/sec. We have not applied these corrections to our measurements.

## III. DATA FROM THE HIGH-PRESSURE ISOMER-SHIFT MEASUREMENTS

The results of our measurements of the pressure dependence of the isomer shift for the element tin[8] are shown in Fig. 1. The results of Panyushkin[11] are also shown. The agreement between his results and ours is within the statistical errors.

A weighted least-squares fit of a straight line was made to our five lowest pressure $S(P)$ points for the lower-pressure Sn-I phase,[4] and to six of our points for the higher-pressure Sn-II phase.[4] These points are well described by

$$S(P)=S(0)+(dS/dP)_0 P \ . \tag{3a}$$

For the lower-pressure or Sn-I phase, and for our five points at or below 62 kbar, the fit gave

$$S(0)=2.508\pm0.006 \ \text{mm/sec} \ , \qquad (dS/dP)_0=-0.00177\pm0.00022 \ \text{mm/sec/kbar} \ . \tag{3b}$$

For the Sn-II phase, and for our six points at or between 124 and 230 kbar, our measurements gave

$$S(0)=2.728\pm0.019 \ \text{mm/sec} \ , \qquad (dS/dP)_0=-0.000243\pm0.000095 \ \text{mm/sec/kbar} \ . \tag{3c}$$

We wish to obtain the value for the change in the isomer shift across the 92 kbar phase transition $\Delta S(92)$. From the isomer-shift results given in Fig. 1, including the results of Panyushkin,[11] we obtain

$$\Delta S(92)=0.32\pm0.02 \ \text{mm/sec} \tag{4}$$

for this change in the isomer shift. We will use this result to obtain a value for the Mössbauer isomer-shift calibration constant $\alpha$ of Eqs. (1).

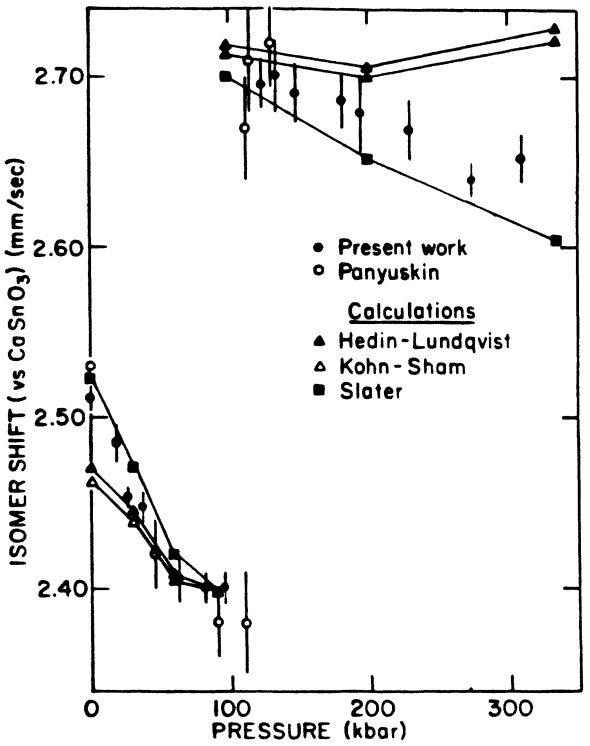


FIG. 1. This figure shows the measured Mössbauer isomer shift for tin as a function of pressure for $0 \leq P \leq 310$ kbar. The data shown include our measurements and those due to Panyushkin (Ref. 11). The figure also shows the results of our calculations of the tin isomer shift, see text and Table I. In these calculations, the electron density at the center of the tin nucleus was calculated by the RAPW method for the Kohn-Sham, the Hedin-Lundqvist, and the Slater treatments of the electron many-body interaction. It was found that, for the change of phase at 92 kbar, the calculated change of electron density at the tin nucleus had only a weak dependence on which of these three descriptions of the many-body interaction was used. Using this fact, together with the measured change of the isomer shift across the phase transition, it was possible to obtain a value for the Mössbauer isomer-shift calibration constant, $\langle\alpha\rangle=0.072a_0^3$ mm/sec. With this $\langle\alpha\rangle$, we were then able to compare the measured and the calculated pressure dependences of the isomer shift for tin for pressures away from the phase transition (see text). The lines which connect the calculated points are there to lead the eye.

## IV. CALCULATIONS OF THE ELECTRON DENSITY AT THE NUCLEUS

The results of our RAPW calculations[8] of the electron density at the tin nucleus are given in Table I, and the calculated $S(P)$ are compared with the above isomer-shift

TABLE I. Electron density at the tin nucleus $\rho_P(0)$ calculated as a function of pressure in a RAPW model using a KS, HL, or SR model for the electron-electron interaction. See text Secs. IV C and IV F. To obtain an electron density, add the number from column 1 to a number in the same row from columns 2–8.

| | Pressure (kilobars) | | | | | | |
|---|---|---|---|---|---|---|---|
| | 0 | 30 | 60 | 90 | 98 | 200 | 335 |
| | Wigner-Seitz radius (atomic units) | | | | | | |
| | 3.512 | 3.451 | 3.398 | 3.353 | 3.337 | 3.263 | 3.185 |
| | Electron density at the nucleus, $\rho_P(0)$, (atomic units) (Kohn-Sham) | | | | | | |
| | Core | | | | | | |
| 190 434.619 | 0.000(5) | 0.224(5) | 0.443(5) | 0.651(5) | 0.801(5) | 1.198(5) | 1.664(5) |
| | Valence | | | | | | |
| 77.86 | 0.00(5) | −0.53(5) | −1.24(5) | −1.60(5) | 2.88(10) | 2.26(10) | 2.22(10) |
| | Total | | | | | | |
| 190 512.48 | 0.00(5) | −0.31(5) | −0.80(5) | −0.95(5) | 3.69(10) | 3.46(10) | 3.89(10) |
| | Electron density at the nucleus, $\rho_P(0)$, (atomic units) (Hedin-Lundqvist) | | | | | | |
| | Core | | | | | | |
| 190 438.611 | 0.000(5) | 0.223(5) | 0.442(5) | 0.648(5) | 0.799(5) | 1.199(5) | 1.664(5) |
| | Valence | | | | | | |
| 78.81 | 0.00(5) | −0.58(5) | −1.32(5) | −1.75(5) | 2.72(10) | 2.06(10) | 1.97(10) |
| | Total | | | | | | |
| 190 517.42 | 0.00(5) | −0.35(5) | −0.88(5) | −1.10(5) | 3.52(10) | 3.26(10) | 3.63(10) |
| | Electron density at the nucleus, $\rho_P(0)$, (atomic units) (Slater) | | | | | | |
| | Core | | | | | | |
| 191 750.511 | 0.000(5) | 0.185(5) | 0.369(5) | 0.546(5) | 0.688(5) | 1.026(5) | 1.441(5) |
| | Valence | | | | | | |
| 86.78 | 0.00(5) | −0.93(5) | −1.79(5) | −2.38(5) | 1.85(10) | 0.84(10) | −0.28(10) |
| | Total | | | | | | |
| 191 837.29 | 0.00(5) | −0.74(5) | −1.42(5) | −1.84(5) | 2.54(10) | 1.87(10) | 1.16(10) |

measurements in Fig. 1. As we will describe below, the calculated results include contributions due to the core electrons.

In Fig. 1, three RAPW curves for $S(P)$ are shown. These RAPW curves correspond to approximate descriptions of the electron many-body interaction in terms of the KS, HL, or SR models. Apart from this difference in the treatment of many-body effects, the three calculations, Table I and Fig. 1, were made by the same RAPW computer programs.

The RAPW programs which we have used for the calculation of $S(P)$ were developed by Krakow[17] and Josephson[18] who used the RAPW energy-band treatment described by Loucks[32] as their starting point. We would like to sketch some of the details of our calculations here.

In these calculations we have specified, in Sec. IV A, the nuclear charge, radius, and surface thickness parameters for a finite tin nucleus, and in Sec. IV B the crystal structure and lattice parameters of tin as a function of pressure. In Sec. IV C, the several models which we have used for the description of the electron-electron interaction are outlined, and in Sec. IV D, the muffin-tin potential used is described. Otherwise, apart from the description of the electron-electron interaction in Sec. IV C, the calculated electron densities follow from the same RAPW computer programs.[17,18,32]

### A. Description of the finite tin nucleus

The nuclear charge density distribution $\rho_n(r)$ used in these calculations is described by a Fermi distribution,

$$\rho_n(r)=K\{1+\exp[(r-r_0)/s]\}^{-1}\ . \tag{5}$$

The nuclear half density radius was taken to be $r_0=5.3324$ fm, and the surface thickness parameter was taken to be $s=0.5666$ fm. $K$ is a constant which was obtained by the normalization of $\rho_n(r)$, Eq. (5), to $50e$, the total positive charge on a Sn nucleus.

### B. Tin crystal structure as a function of pressure

We need information about the crystal structure of tin as a function of pressure, below, in connection with RAPW calculations of $S(P)$. An x-ray diffraction study of the crystal structure and of the $T,P$ phase diagram of tin has been made by Barnett *et al.*[4] Their measurements were made for the pressure range $0\leq P\leq 100$ kbar, and for temperatures in the range $298\leq T\leq 773$ K. Their pressure measurements were based on measurements of the lattice parameter of NaCl.

For a temperature of 298 K, in the pressure range $0\leq P\leq 92$ kbar, they found tin to have a body-centered tetragonal structure with two atoms in the unit cell. This

is referred to as the Sn-I phase. They found the phase transformation to a higher pressure Sn-II phase to be at 92 kbar. Sn-II has a body-centered tetragonal structure with a basis of but one atom in the unit cell. In the Sn-II phase they described two structure measurements made at 93 and 98 kbar.

In their study of the phase diagram, they found that along the phase boundary between Sn-I and Sn-II, in the Sn-II phase, the $c/a$ ratio of the tetragonal cell was constant within experimental error over the pressure range from 39 to 98 kbar. No detailed crystal structure data are available above 98 kbar.

In order to continue our RAPW calculations of $S(P)$ into the Sn-II phase to 310 kbar, we have calculated the volume of the tin unit cell as a function of pressure from the shock-wave data of Walsh *et al.*[2] and of Al'tshuler *et al.*[3] In the absence of any other information, we observe that neither the unit-cell volume as a function of $P$, nor our $S(P)$ measurements, suggest a change of phase for Sn between 98 and 310 kbar. The fact that Barnett *et al.*[4] found $c/a$ for Sn-II to be independent of $P$, within error, along the phase boundary between Sn-I and Sn-II from 39 to 98 kbar may indicate that $c/a$ has only a weak dependence on $P$ for $T=298$ K and in our higher-pressure Sn-II region.

At 298 K, in the pressure range of Barnett *et al.*[4] from 0 to 98 kbar, we have used their x-ray diffraction data to obtain the crystal structure and lattice parameters of tin. For the higher-pressure region, $98 \leq P \leq 310$ kbar, where structure data are not otherwise available, we have used the results of Walsh *et al.*[2] and of Al'tshuler *et al.*[3] to obtain the size of the unit cell, and we have assumed tin to have a body-centered tetragonal unit cell with a one atom basis like that found by Barnett *et al.*[4] at 98 kbar. We have taken the unit cell to have the same ratio, $c/a=0.911$, as that which they found for Sn-II at 98 kbar, and we have assumed this $c/a$ to be independent of $P$ for the region 98—310 kbar. We will assume the NaCl pressure scale used by Barnett *et al.*[4] to be the same as the ruby fluorescence scale of Mao *et al.*[29] which we have used.

### C. Many-body potentials

The many-body local potentials $V_i(r)$ which we have used are described by

$$V_i(r) = -J[(3/\pi)\rho_P(r)]^{1/3} , \tag{6a}$$

where from Slater[21]

$$J=3/2 ,$$

from Kohn-Sham[19] (6b)

$$J=1 ,$$

and from Hedin-Lundqvist[20]

$$J=J(x) , \tag{6c}$$

with

$$J(x)=1+Bx\ln[1+(1/x)] ,$$

and with

$$B=0.7734, \quad x=r_s/21 ,$$

and

$$r_s=\{3/[4\pi\rho_P(r)]\}^{1/3} ,$$

where $\rho_P(r)$ is the total electron density at $r$ and at the pressure $P$.

Equations (6) are examples of many-body potentials which have been of interest. The Slater and the Kohn-Sham potentials may represent extremes of potentials of this kind. Our present purpose is to compare these and the Hedin-Lundqvist potential with our high-pressure Mössbauer data. In the present study of the sensitivity of $S(P)$ for tin to the description of exchange and correlation, we may regard these potentials as covering a range of strengths. In this context, the SR potential is the strongest, and the Kohn-Sham potential the least strong of the three.

### D. Dirac-Hartree-Wigner-Seitz muffin-tin potential

In RAPW band-structure studies, calculations have sometimes been based on an initial potential for the component atoms of the solid which was obtained from a solution of the Dirac equation, and in which free-atom boundary conditions were used. The solution to the Dirac equation was usually obtained in a self-consistent way, subject to certain constraints. This initial free-atom potential was then suitably modified to obtain the required muffin-tin potential.[32]

In the present RAPW calculations, we have obtained an initial potential for the tin atom through the use of the DHWSXC model. This procedure has much similarity to the above method. In the DHWSXC model,[15] the solution to the Dirac equation for the component atoms of the solid is also self-consistent within similar constraints. The essential difference is that, in the DHWSXC model, the wave functions and a total potential are obtained within the finite volume $V(P)$ of the appropriate Wigner-Seitz sphere, of radius $R_{WS}(P)$, rather than for free-atom boundary conditions in infinite space. Thus, the volume per atom, or $1/V(P)$, which is the essential variable of this study of $S(P)$, is introduced through the initial potential at the first stage of the RAPW calculation. This DHWSXC total potential was modified to obtain a muffin-tin potential, as we will describe below.

We would like to describe some details of the DHWSXC computer program here. For greater detail, the reader is requested to refer to the DHWSXC paper, Ref. 15. This program treats the atomic many-body problem in a self-consistent field approximation. The Dirac equation is used to describe the motion of the individual electrons. The self-consistent potential is chosen to be of the Hartree type and provision is made for incorporating exchange and correlation in the form of a local potential. The local potential used was the KS, HL, or SR model as described by Eqs. (6) above.

In a calculation of the wave functions and of the total potential for an atom in this DHWSXC model, the

Wigner-Seitz radius as a function of pressure $R_{WS}(P)$, and the electron configuration of the atom must be specified. Here

$$R_{WS}(P)=[3V(P)/4\pi]^{1/3},$$

where $V(P)$ is the volume per tin atom in the solid at the pressure $P$. A tabulation of the $R_{WS}(P)$ used is given in Table I. In the following RAPW calculations for tin, the DHWSXC total potential has been obtained for a $4d^{10}$ core and an assumed $5s^2_{1/2}5p^2_{1/2}$ valence electron configuration. The slope of the large component of each of the Dirac wave functions for the specified tin configuration is required to be zero on this WS spherical surface at $R_{WS}(P)$.

The wave functions around the origin, at $r=0$ and for the first few percent of the nuclear radius, were obtained through an analytic integration of the Dirac equation. Beginning with these analytic results, a numerical calculation of the wave functions and of the total DHWSXC potential was made at 249 radial points. The innermost point for the numerical integrations was at a radius which was a few percent of the nuclear radius $r_0$, and the outer point was at the Wigner-Seitz radius $R_{WS}(P)$.

These DHWSXC calculations were made to a self-consistency of a few parts in $10^9$ for all of the wave functions, for the total potential, and for the eigenvalues. Evidence for this self-consistency may be seen in the similar behavior of the core electron densities at the nucleus for the KS and HL models shown in Table I. In that 50 electrons have been included in the configuration for tin, the total potential is that for a neutral tin atom.

For each pressure, and corresponding atomic volume $V(P)$ for tin, this program yielded wave functions and a total DHWSXC potential which, within the constraints indicated, are self-consistent including the core states. This total potential has spherical symmetry.

In the construction of the muffin-tin (mt) potential, the radius of the muffin tins $r_{mt}$ was selected so that nearest-neighbor muffin tins were in contact. The potential within the muffin-tin radius was taken to be that obtained in the above DHWSXC calculation. In the region exterior to the muffin tins, the potential was taken to be a constant equal to the average value of the DHWSXC potential from $r_{mt}(P)$ to $R_{WS}(P)$. In this model, a contribution from the many-body potential is thus included in this exterior region. As is usual in APW and RAPW calculations, there is a step in the muffin-tin potential at $r_{mt}$. A value for this step was obtained in the above calculation.

The DHWSXC treatment of the atom provides a way to obtain a RAPW muffin-tin potential, and a set of core wave functions, which within the constraints indicated, have a self-consistency, and which also reflect the decrease of the Sn atomic volume as pressure is applied to the tin metal. One can then obtain an estimate of the pressure dependent contributions to $S(P)$ due both to the valence (RAPW) and to the core (DHWSXC) electrons.

### E. A value for $g$

In Eqs. (1), we need the value for $g$, the ratio of the electron density averaged over the nuclear volume to this density at $r=0$. Because the nuclear potential is dominant near $r=0$, $g$ will be nearly the same for the above DHWSXC valence $s$ states and for the RAPW valence-band states. From the above DHWSXC $5s$ wave functions, we obtain $g=0.975$ for tin.

### F. Details of the RAPW calculation

In the RAPW method,[32,34] the wave functions are decomposed in terms of the angular-momentum quantum number $\kappa$ inside of the muffin-tin radius, and in terms of reciprocal-lattice vectors (RLV) outside. In the results given in Table I and in Fig. 1, $\kappa$ was truncated at $\kappa=8$ and 50 RLV's were used. The 50 RLV's were chosen from a larger set as the 50 vectors closest to the point $\bar{k}$ in $\bar{k}$ space for which the calculation was being performed.

Several tests of the convergence of the eigenvalues were carried out for both the $\kappa$ and the RLV expansions. The change in the eigenvalue for the point at the center of the Brillouin zone was found to be about $10^{-4}$ Ry when the maximum value of $|\kappa|$ was increased from 5 to 10, and also for an increase in the number of RLV's from 50 to 98. We estimate that an error of this magnitude in the eigenvalues will lead to numerical errors in the calculated $S(P)$ that are small compared to our experimental errors.

Calculations of energy eigenvalues were made at 75 $\bar{k}$ points on an array of uniform density in an irreducible part of the first Brillouin zone. This irreducible part has a volume which is $\frac{1}{16}$ of the volume of the first zone. 50 of these $\bar{k}$ points were entirely within this volume and, in following calculations, had a weight of one, while 25 $\bar{k}$ points were on an interface between two such volumes and had a weight of 0.5. Thus there were, effectively, 62.5 $\bar{k}$ points associated with this volume, or 1000 $\bar{k}$ points in the first Brillouin zone.

Eigenvalues were calculated through an energy region of about 1 Ry beginning at an energy slightly below the bottom of the band and extending well above the Fermi surface. For the above $\frac{1}{16}$ of the first zone, and for Sn-I at 30 kbar, for example, 343 eigenvalues were found. These roots and their corresponding $\bar{k}$ vectors were ordered according to increasing energy.

In the reduced zone scheme, and for 1000 $\bar{k}$ points in the zone, each $(E,\bar{k})$ point will correspond to $2\times10^{-3}$ electron. In the Sn-I phase, with two atoms in the primitive unit cell, one must account for eight electrons, and for the Sn-II phase, with one atom in the primitive cell, one must account for four electrons. Thus the Fermi energy will be in the vicinity of the 4000th root for Sn-I and near the 2000th root for Sn-II in the above ordered sequences of the $(E,\bar{k})$ states.

At each of the above $(E,\bar{k})$ states at or below the Fermi level, the normalized RAPW wave function was then obtained and the electron density at a tin nucleus for this state was calculated. An estimate of the electron density at the Sn nucleus due to the valence band was then obtained by summing the individual densities for these $(E,\bar{k})$ states below the Fermi level. We estimate that the numerical error in the RAPW valence electron densities given in Table I, due to this approximate integration over the Brillouin zone, is about $0.05a_0^{-3}$ for Sn-I and $0.1a_0^{-3}$ for Sn-II. There is a small scatter of the calculated points

for $S(P)$ in Fig. 1, which comes mostly from this approximate integration.

The electron densities at the nucleus given in Table I are values calculated at $r=0$. The total values given there for the core states are sums of the values for the core $s_{1/2}$ and $p_{1/2}$ levels obtained in the Dirac-Hartree-Wigner-Seitz-XC model, while the densities due to the valence bands were those obtained from the above RAPW-model calculations. The total electron density at the nucleus as a function of pressure, including all of the core and valence states, is given in Table I, and is described by $\rho_P(0)$.

## V. PROPERTIES OF THE CALCULATED MÖSSBAUER ISOMER SHIFT $S(P)$

When graphs of the calculated total electron density at the nucleus, $\rho_P(0)$, were made versus pressure, it was found, as expected, that these total densities increased in going from the Kohn-Sham to the Hedin-Lundqvist to the Slater model for the description of the many-body electron interaction. The Mössbauer effect cannot measure the total electron density at the nucleus, however, but it can give a measure of changes in this density.

### A. The Mössbauer isomer-shift calibration constant $\alpha$

We have used the calculated change of this electron total density across the 92-kbar phase transition $\Delta\rho_{92}(0)$ together with $\Delta S(92)$, Eq. (4), to obtain a value for the Mössbauer isomer-shift calibration constant of Eqs. (1b) and (1c). The three calculated values for $\Delta\rho_{92}(0)$, in atomic units, Table I, are 4.64, 4.62, and $4.38a_0^{-3}$, where $a_0$ is the first Bohr radius. With $g=0.975$, these results give values for $\alpha$ of 0.071, 0.071, and $0.075a_0^3$ mm/sec. These three values for $\alpha$ are somewhat different in nature in the sense that they are based on different models for the electron many-body interaction. In comparison with our experimental errors in the measurement of $S(P)$, however, they will be seen to cluster fairly closely. In order to display this clustering clearly, and in order to compare the calculated $\rho_P(0)$ for the KS, HL, and SR models with the measured $S(P)$ in Fig. 1, we need to select a specific $\alpha$ value. For this purpose of comparison and display, we have used the average of the above three $\alpha$ values, viz.,

$$\langle\alpha\rangle=0.072a_0^3 \text{ mm/sec} . \tag{7}$$

We have not given an error for this $\langle\alpha\rangle$ value for we have no adequate estimate, for example, of the errors intrinsic to the RAPW model. If all of the error were associated with the measurement of $\Delta S(92)$, Eq. (4), the error for $\langle\alpha\rangle$ would be $\pm0.005a_0^3$ mm/sec.

The average $\langle\alpha\rangle$, Eq. (7), is quite close to the value $0.0726a_0^3$ mm/sec given by Antoncik,[14] but is less than the value obtained by Roggwiller and Kundig,[35] $\alpha=0.0925\pm0.01a_0^3$ mm/sec. If we were to suppose an error of about 10% in our calculated electron densities at the nucleus, the error bars for our $\langle\alpha\rangle$ and for the Roggwiller and Kundig $\alpha$ value[35] would overlap. We have used $\langle\alpha\rangle$ of Eq. (7) in Eqs. (1b) and (1c) in the comparison of the calculated $\rho_P(0)$ of Table I with the measured $S(P)$ in Fig. 1.

A value for the nuclear size change $\Delta\langle r^2\rangle$ can be obtained from the value for $\langle\alpha\rangle$ of Eq. (7) and from the formula for the isomer shift, Eqs. (1). We obtain

$$\Delta\langle r^2\rangle=0.0055 \text{ fm}^2 . \tag{8}$$

Either the Antoncik or the Roggwiller and Kundig $\alpha$ value would give a quite similar value for $\Delta\langle r^2\rangle$.

We note that the value for the Mössbauer isomer-shift calibration constant $\langle\alpha\rangle$ is obtained from the measured change of the isomer shift across the 92-kbar phase transition, and that this $\langle\alpha\rangle$ is then used in the comparison of the calculated $S(P)$ with the measured $S(P)$ data for pressures away from the phase transition. The experiment is thus internally calibrated, and, in a sense, we compare the step of the isomer shift at the phase transition with the behavior of $S(P)$ for other regions of $P$.

### B. The reference pressure $Q$

Since the Mössbauer effect does not measure the total electron density at the nucleus, but only changes in this quantity, we may subtract suitable densities from the densities given in Table I such that the calculated $S(P)$ for the KS, HL, and SR models may be fitted to the measured $S(P)$ at one selected pressure value. We have chosen to fit the three calculated $S(P)$ curves to the measured data at 90 kbar. This is the reference pressure, $Q=90$ kbar, of Eq. (1c). In this way, the clustered values of the calculated $\Delta S(92)$ at the phase transition, for the KS, HL, and SR models, have been displayed and compared with the measured $S(P)$ in Fig. 1.

Because of this curve-fitting procedure, the calculated 90-kbar point $S(90)$ acts as a kind of "pivot-point". The curve calculated for the Slater model lies above the KS and HL curves below 90 kbar, but lies below the latter two curves for pressures above 90 kbar. The $S(P)$ curves calculated for the KS and HL models group relatively closely together.

### C. Calculated slope of $S(P)$: Comparison of RAPW and DHWSXC models

The $[S(90)-S(0)]$ in Sn-I and $[S(335)-S(98)]$ in Sn-II, calculated in the RAPW model, Table I and Fig. 1, are found to be increasingly negative the stronger the many-body potential, viz., for the sequence of interactions, KS, HL, to SR.

In earlier studies,[5-7] as described in Sec. I, we found that $[dS(P)/dP]_0$ calculated in the DHWSXC spherical model was sensitive to the potential, Eqs. (6), used to describe the many-body interaction. For the DHWSXC model also, $[dS(P)/dP]_0$ was found to be increasingly negative for this sequence of interactions, KS, HL, to SR.

Our present RAPW calculations of $S(P)$ are based on DHWSXC muffin-tin potentials. Our earlier DHWSXC and the present RAPW calculations of $S(P)$ are thus related, and the results for $S(P)$ and for $[dS(P)/dP]_0$ for the DHWSXC and RAPW models are found to have a qualitative similarity. The DHWSXC model cannot describe the 92-kbar phase transition, but, in the RAPW

model, a description of $\Delta S(92)$ for the phase transition is obtained.

Although the valence contribution is dominant, Table I, the core and the valence electrons are found in the model to make comparable contributions to the slope of $S(P)$. These contributions tend to be of opposite sign. With increasing $P$, the core electrons move toward, and the valence electrons away from the nucleus. Because the core and valence electron contributions are found to be comparable, $S(P)$ for tin must be calculated in all-electron treatment, as we have done in an approximate way here.

### D. $(E,\bar{k})$ dependence of the slope of $S(P)$, and the ground state

We have calculated the pressure derivative of the electron density at the nucleus near zero applied pressure $[d\rho(E,\bar{k},P,r)/dP]_0$ at $r=P=0$ for each of the individual $(E,\bar{k})$ points obtained above in eigenvalue calculations for the irreducible part of the Brillouin zone. We find that this density derivative is less than zero for $(E,\bar{k})$ states near the bottom of the band structure, but is greater than zero for states near the Fermi surface.[7,8]

Our result that the derivative $[d\rho(E,\bar{k},P,r)/dP]_0>0$ for states near the Fermi surface is in qualitative accord with the Knight-shift measurements of Matzkanin and Scott.[36] In that our present treatment of the Fermi surface is not sufficiently detailed, we have not sought to make a calculation of the Knight-shift result here.

In an integral of the above $[d\rho(E,\bar{k},P,r)/dP]_0$ over the band states at and below the Fermi level to obtain an RAPW value for $[dS(P)/dP]_0$, the positive contributions from the states in the upper region of the band will cancel with negative contributions from some of the states in the lower part of the band structure, and the dominant contribution to $[dS(P)/dP]_0$, which is negative, Eqs. (3), will be found to be due to states in the lower region of the band. In this way, one may understand the qualitative similarity of the $[dS(P)/dP]_0$ calculated in the RAPW and DHWSXC models. The energies of the DHWSXC model states and of the RAPW states at the bottom of the band are similar, and, in both models, $[dS(P)/dP]_0$ is due to this ground-state energy region. The RAPW model gives a much better description of the measured $S(P)$ and of $[dS(P)/dP]_0$, but the DHWSXC model for the ground-state region gives appreciably similar results to those of the RAPW model.

### E. Is the slope of $S(P)$ "large" or "small"?

In Sec. I, we have suggested that the slope of $S(P)$ was "small" or comparable to the changes of $[dS(P)/dP]_P$ for the sequence of many-body potentials, KS, to HL, to SR. For both the earlier DHWSXC work, and the results of the present RAPW calculations shown in Fig. 1, this is found to be the case.

We may compare the percentage change of the valence electron density at the tin nucleus to the percentage change of the bulk density as the pressure is increased. From Table I, the calculated valence electron density at the nucleus is near $80a_0^{-3}$ at zero pressure. When the pressure is increased to 335 kbar, this density decreases by about $2a_0^{-3}$ or less, a change of a few percent. On the other hand, the bulk density has increased by over 30% for this pressure range. This behavior is a strong departure from that of a free-electron gas, but is qualitatively like the result suggested by the DHWSXC model, Sec. I. In this sense also, we may say that the slope of $S(P)$ with increasing $P$ is small for tin. In contrast to tin, for metallic gold near zero applied pressure, the electron density at the nucleus is approximately proportional to the bulk metallic density.[26]

### F. Existence of a minimum in $S(P)$ as a function of $P$

Earlier estimates of $S(P)$ for Sn which we have made in the DHWSXC model[5-7] suggested that in the vicinity of 300 to 600 kbar, $S(P)$ would have a minimum, Sec. I, and begin to increase, rather than to decrease, for a further increase of $P$. Apart from the increase of $S(P)$ at the 92-kbar phase transition, the results of Fig. 1 show that the measured $S(P)$ decreases with increasing $P$ in both the Sn-I and the Sn-II phase, and is still decreasing with increasing $P$ near 310 kbar. A minimum in $S(P)$ was not found within our pressure range.

### G. Self-consistency

Our RAPW calculations have not been made fully self-consistent[37,38] for the core and valence-band electrons. Our present RAPW calculations of $S(P)$ have a degree of self-consistency, however. This is due to the fact that the muffin-tin potential and the core wave functions, on which the calculations are based, were obtained from the DHWSXC model. Within the constraints indicated, the DHWSXC model is self-consistent for all electrons within the entire atomic or WS volume $V(P)$ that is appropriate to tin at the particular pressure $P$.

### H. Use of $S(P)$ measurements in the study of the many-body interaction

The results of Fig. 1 show that, in our present application of the RAPW model, the differences between the $S(P)$ curves calculated for the KS, HL, and SR models are comparable to or larger than our experimental errors in the measurement of $S(P)$ and of $[dS(P)/dP]_0$ for both tin phases. These differences are found to increase as the calculations are extended to higher pressures and Sn electron densities.

Within the limits of our present study, these results indicate that the slope of $S(P)$ for Sn is sensitive to the strength of the potential used to describe many-body effects. In comparing the calculations with experiment, the effective, or useful, sensitivity will be greater, the wider the pressure range covered by the measurements and calculations. This sensitivity may be helpful in further studies of the KS, HL, SR, and possibly other models for the electron many-body interaction.

#### *1. The many-body potential, $V_i(r)$*

In comparing the three calculated $S(P)$ curves with the experimental data in Fig. 1, the curve for the SR model is found to fall somewhat closer to the measured points than

the curves for the KS or HL models. This agreement is fairly close for pressures at and below the phase transition. Above the phase transition, all three calculated curves depart from the experimental data to an increasing extent.

We have given arguments above that the relative slopes of the calculated $S(P)$ curves are sensitive to the description of exchange and correlation used in the calculations. The slopes of all three curves for $S(P)$ will also be affected together, simultaneously, to some degree by the approximations made in the RAPW band-structure model.

It is usually expected that the KS or HL model should give a better description of band-structure properties than the SR model. The fact that the SR model gives a somewhat better agreement with experiment than the other two interactions considered here may be related to the fact that the RAPW band-structure model is itself approximate in nature.[37,38]

## VI. OTHER RESULTS

Insofar as we are aware a muffin-tin potential, constructed from a DHWSXC potential, has not been explored previously in band-structure studies. In Fig. 2 we show the energy band structure for tin for a pressure of 30 kbar. These curves were calculated with the Slater interaction from a DHWSXC–muffin-tin potential. The energy bands obtained are quite similar in structure to results which have been obtained previously by Craven[39] who used an empirical pseudopotential method, and by Ament and Vroomen[40] who used the RAPW method. Our determination of the Fermi energy is relatively crude.

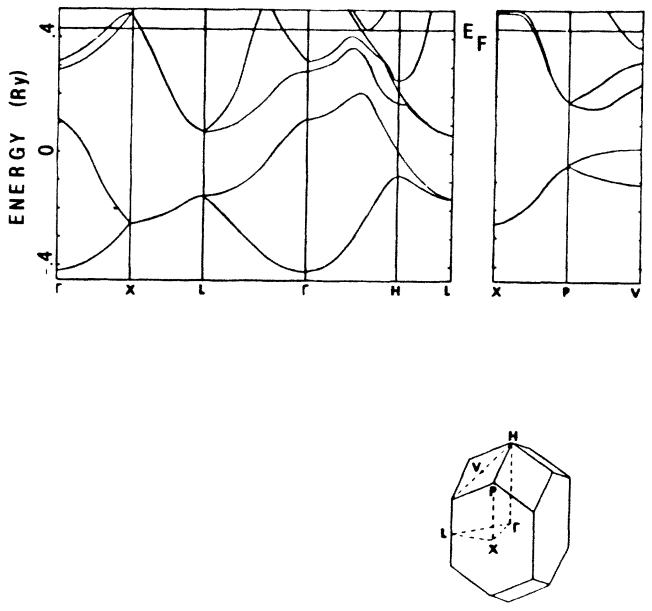


FIG. 2. The upper curves show the calculated energy band structure for tin in high-symmetry directions. These RAPW calculations were made with the Slater treatment of the many-body interaction, for Sn-I at a pressure of 30 kbar. The lower part of the figure shows the Sn-I Brillouin zone and indicates the high-symmetry points and directions (see text).

We note, however, that we obtain a Fermi energy of 0.82 Ry for the KS interaction at zero applied pressure. This may be compared to the value found by Craven of 0.77 Ry and to that obtained by Ament and Vroomen of 0.83 Ry. Our value, which is also based on the RAPW method, is close to the latter result.

The electron density ratio $\rho_{5s}(0)/\rho_{4s}(0)$ has been measured by Bocquet *et al.*[41] by conversion electron spectroscopy. They obtained a value for this ratio of $0.108\pm0.003$. Using the DHWSXC model to find $\rho_{4s}(0)$ and the RAPW model to find $\rho_{5s}(0)$, we obtain values for this ratio of 0.100, 0.101, and 0.109, respectively, for the KS, HL, and SR models. The range of our calculated values is comparable to the error in the measurement of this ratio but perhaps the SR model is somewhat favored. This would be consistent with the results of Table I and Fig. 1.

## VII. SUMMARY

A measurement of the Mössbauer isomer shift $S(P)$ has been made for the element tin as a function of pressure for the range $0\leq P\leq 310$ kbar. The bulk density of tin increases by about 30% for this pressure range. RAPW calculations of the electron density at the nucleus have been made for this range of pressure. In these calculations the electron-electron interaction was described in the Kohn-Sham, the Hedin-Lundqvist, or the Slater model.

It was found that the calculated change of electron density at the nucleus across the 92-kbar phase transition, in comparison with our experimental errors, had only a weak dependence on which of these models was used to describe the electron many-body interaction. Thus a value for the Mössbauer isomer-shift calibration constant $\langle\alpha\rangle = 0.072a_0^3$ mm/sec was obtained. This value is independent, within a few percent, of the model KS, HL, or SR, used to describe many-body effects. This $\langle\alpha\rangle$ is in fair agreement with other recent results for $\alpha$. With this value for $\langle\alpha\rangle$, it was possible to compare the RAPW calculations of $S(P)$ with the isomer-shift measurements as a function of pressure.

Because $\langle\alpha\rangle$ is obtained from the change of the isomer shift of tin at the phase transition, the experiment is internally calibrated. Thus, in a sense, we compare the change of isomer shift across the phase transition with the behavior of $S(P)$ at other pressures.

Complete crystal-structure data are not available for our entire pressure range, but, using the information that is available, the RAPW-DHWSXC model provides an approximate description of the measured $S(P)$. We find that, away from the phase transition, this calculated isomer shift has a significant dependence on the model used to describe many-body effects. The RAPW-DHWSXC calculations are also compared with some other measurements and observations.

For our approximate RAPW-DHWSXC calculation, the $S(P)$ curve calculated in the Slater model falls somewhat closer to the data than the other curves. In making further, possibly fully self-consistent calculations of $S(P)$, additional crystal-structure data for the high-pressure Sn-II phase would be most helpful. Because core and valence electron contributions to $S(P)$ are found to be of similar

magnitude, a further calculation of $S(P)$ for tin should be fully self-consistent for all of the electrons. Because $S(P)$ depends on the electron density near the nucleus where electron velocities approach the velocity of light these self-consistent calculations must be fully relativistic.

## ACKNOWLEDGMENTS

We would like to express our appreciation to Dr. P. M. Bell and to Dr. G. J. Piermarini for introducing us to diamond-clamp high-pressure technology, and to Dr. Kien Dy and to Dr. W. J. Thompson for many helpful discussions of the several aspects of this work. This work was supported by the National Science Foundation under Grant No. DMR-78-18915 to the University of North Carolina, and by grants from the University Research Council of the University of North Carolina. The work of J. N. F. was submitted in partial fulfillment of the requirements for the degree of Doctor of Philosophy at the University of North Carolina.

---

*Present address: Department of Physics, University of Central Florida, Orlando, FL 32816.

†Present address: Bell Laboratories, 555 Union Blvd., Allentown, PA 18103.

‡Present address: Los Alamos National Laboratory, Mail Stop K764, University of California, Los Alamos, NM 87545.

[1]H. Frauenfelder, *The Mössbauer Effect* (Benjamin, New York, 1962).

[2]J. M. Walsh, H. M. Rice, R. G. McQueen, and F. L. Yarger, Phys. Rev. **108**, 196 (1957).

[3]L. V. Al'tshuler, K. K. Krupnikov, and M. I. Brazhnik, Zh. Eksp. Teor. Fiz. **34**, 886 (1958) [Sov. Phys.—JETP **7**, 614 (1958)].

[4]J. D. Barnett, V. E. Bean, and H. F. Hall, J. Appl. Phys. **37**, 875 (1966).

[5]D. L. Williamson, John H. Dale, W. D. Josephson, and Louis D. Roberts, Phys. Rev. B **17**, 1015 (1978).

[6]William T. Krakow, William D. Josephson, P. A. Deane, Don L. Williamson, and Louis D. Roberts, Phys. Rev. B **23**, 499 (1981).

[7]Coin T. Page, John H. Dale, Lee Chow, Joseph N. Farrell, William D. Josephson, and Louis D. Roberts, Phys. Rev. B **27**, 6037 (1983).

[8]Joseph N. Farrell, Ph.D. thesis, University of North Carolina, 1984.

[9]H. S. Möller, Z. Phys. **212**, 107 (1968).

[10]H. S. Möller and R. L. Mössbauer, Phys. Lett. **24A**, 416 (1967).

[11]V. N. Panyushkin, Fiz. Tverd. Tela (Leningrad) **10**, 1915 (1968) [Sov. Phys.—Solid State **10**, 1515 (1968)].

[12]V. N. Panyushkin and F. F. Voronov, Pis'ma Zh. Eksp. Teor. Fiz. **2**, 153 (1965) [JEPT Lett. **2**, 97 (1965)].

[13]J. E. Inglesfield, J. Phys. Chem. Solids **31**, 1443 (1970).

[14]E. Antoncik, Phys. Rev. B **23**, 6524 (1981).

[15]T. C. Tucker, Louis D. Roberts, C. W. Nestor, T. A. Carlson, and F. B. Malik, Phys. Rev. **178**, 998 (1969).

[16]Don L. Williamson, in *Mössbauer Isomer Shifts*, edited by G. K. Shenoy and F. F. Wagner (North-Holland, Amsterdam, 1978).

[17]William T. Krakow, Ph.D. thesis, University of North Carolina, 1978.

[18]W. D. Josephson, Ph.D. thesis, University of North Carolina, 1975.

[19]W. Kohn and L. J. Sham, Phys. Rev. **140**, A1133 (1965).

[20]L. Hedin and B. I. Lundqvist, J. Phys. C **4**, 2064 (1971).

[21]J. C. Slater, Phys. Rev. B **1**, 385 (1951).

[22]*American Institute of Physics Handbook*, 3rd ed. edited by D. E. Gray (McGraw-Hill, New York, 1972).

[23]*Mössbauer Effect Data Index*, edited by J. G. Stevens and V. E. Stevens (IFI/Plenum, New York, 1974).

[24]G. S. Collins and N. Benczer-Koller, Phys. Rev. B **17**, 2085 (1978).

[25]E. N. Kaufman and R. J. Vianden, Rev. Mod. Phys. **51**, 161 (1979).

[26]Louis D. Roberts, D. O. Patterson, J. O. Thomson, and R. P. Levey, Phys. Rev. **179**, 656 (1969).

[27]G. J. Piermarini and S. Block, Rev. Sci. Instrum. **46**, 973 (1975).

[28]A. Jayaraman, Rev. Mod. Phys. **55**, 65 (1983).

[29]H. K. Mao and P. M. Bell, Carnegie Institution Yearbook **76**, 646 (1977).

[30]J. Burton, Oak Ridge National Laboratory Technical report, 1970 (unpublished).

[31]D. J. Erickson, Louis D. Roberts, J. W. Burton, and J. O. Thomson, Phys. Rev. B **3**, 2180 (1971).

[32]T. L. Loucks, *Augmented Plane Wave Method* (Benjamin, New York, 1967).

[33]L. R. B. Elton, *Nuclear Sizes* (Oxford, London, 1961).

[34]Joseph Callaway, *Quantum Theory of Solids* (Academic, New York, 1976).

[35]P. Roggwiller and W. Kundig, Phys. Rev. B **11**, 4179 (1975).

[36]G. A. Matzkanin and T. A. Scott, Phys. Rev. **151**, 360 (1966).

[37]J. C. Slater, *The Self-Consistent Field for Molecules and Solids: Quantum Theory of Molecules and Solids* (McGraw-Hill, New York, 1974), Vol. 4.

[38]H. J. F. Jansen and A. J. Freeman, Phys. Rev. **30**, 561 (1984).

[39]J. E. Craven, Phys. Rev. **182**, 693 (1969).

[40]M. A. E. A. Ament and A. R. de Vroomen, J. Phys. F **4**, 1359 (1974).

[41]J.-P. Bocquet, Y. Y. Chu, O. C. Kistner, M. L. Perlman, and G. T. Emery, Phys. Rev. Lett. **17**, 809 (1966).